P H Y S I C A L   R E V I E W   L E T T E R S

Band Formation in a Molecular Quantum Well via 2D Superatom Orbital Interactions

Daniel B. Dougherty,[1,*] Min Feng,[2] Hrvoje Petek,[2,‡] John T. Yates, Jr.,[1,†] and Jin Zhao[2,3,‡]

[1]*Surface Science Center and Department of Chemistry, University of Pittsburgh, Pittsburgh, Pennsylvania 15260, USA*
[2]*Department of Physics and Astronomy, University of Pittsburgh, Pittsburgh, Pennsylvania 15260, USA*
[3]*Hefei National Laboratory for Physical Sciences at Microscale and Department of Physics,
University of Science and Technology of China, Hefei, Anhui 230026, People's Republic of China*

By scanning tunneling microscopy and spectroscopy, we study nearly free electron band formation of the σ^* lowest unoccupied molecular orbital of C_6F_6 on a Cu(111) surface. In fractal islands, the lowest unoccupied molecular orbital energy systematically stabilizes with the number of interacting near-neighbor C_6F_6 molecules. Density functional theory calculations reveal the origin of effective intermolecular orbital overlap in the previously unrecognized superatom character of the σ^* orbital of C_6F_6 molecules. The discovery of superatom orbitals in planar molecules offers a new universal principle for effective band formation, which can be exploited in designing organic semiconductors with nearly free electron properties.

Molecules provide a myriad of building blocks with potential applications in electronic materials. Electronic band formation with the effective mass approaching that of a free electron in molecular semiconductors is a desirable but elusive property for molecular electronics [1,2]. The primary focus of research on charge transport in organic semiconductors has been on π-conjugated molecules with delocalized intramolecular wave functions, and potential for effective intermolecular coupling [1–5]. The cofacial arrangement of aromatic rings (π stacking) is known to favor strong intermolecular overlap between π orbitals [1,5–7]. Pauli repulsion, however, deters the cofacial arrangement of molecules such as polyacenes in crystalline materials [1,4]. Instead, electropositive H atoms interact with the π-electron charge density [5,8] to impose herringbone structures, forcing a nearly orthogonal π-orbital arrangement among adjacent molecules [1,4]. Because of the unfavorable packing, as well as poor screening and strong electron-phonon interaction, molecular materials fail to achieve the band transport implicit in the pairwise overlap integrals for the π-stacking geometry [1].

Nevertheless, studies of organic molecule-metal interfaces by photoemission spectroscopy and low-temperature scanning tunneling microscopy (LT-STM) offer tantalizing evidence for nearly free electron (NFE) band formation [9–13]. Usually, however, the NFE properties can be attributed to perturbation of the metal surface electronic structure by the molecule-surface interaction [9,11,13–17]. Therefore, it is an open question whether the valence or conduction bands of molecular semiconductors can acquire NFE character through intrinsic intermolecular interactions.

A striking example of intrinsic NFE band formation was discovered for C_{60} quantum wells on metals by two-photon photoemission (2PP) spectroscopy, and LT-STM imaging [12,14]. The physical origin of intermolecular interactions was clarified with the discovery of the superatom molecular orbitals (SAMOs) of hollow molecules [12]. SAMOs are diffuse atomlike orbitals where the central exchange correlation and dipole potentials bind electrons to the nonnuclear regions in the hollow molecular core and outer perimeter rather than to individual atoms [12,18–21]. Because of their diffuse nature, the s-symmetry SAMOs in C_{60} quantum structures hybridize into dispersive bands possessing an effective mass, $m_{\rm eff}$ of $1.4m_e$ and minima at 3.3–3.6 eV above the Fermi level (E_F) [14,22]. The facile relaxation to lower energy LUMO states, however, prevents SAMOs derived bands of C_{60} from mediating electron transport [14,23]. Although strategies for stabilizing SAMOs have been proposed [18,24], so far no molecular semiconductor with a SAMO derived conduction band has been identified.

Other intriguing examples of molecular NFE band formation have been reported in 2PP and photoemission spectroscopy for the $4a_{1g}\sigma^*$ LUMO and occupied $2a_{1g}\sigma$ orbitals of C_6F_6 [9] and C_6H_6 [25], respectively, on metal surfaces. It remains unclear why these oblate molecules lying flat on metal surfaces and interacting through weakly polarizable atoms achieve strong wave function overlap. To answer this question, in this Letter we explore the physical origin of the NFE band formation within fractal C_6F_6 islands on Cu(111) surface by molecule-resolved LT-STM and density functional theory (DFT). LT-STM probes the real-space intermolecular interactions through energy stabilization of the σ^* state as the number of near-neighbor C_6F_6 molecules increases, which is implicit in the energy-parallel momentum dispersion of the LUMO band in 2PP spectra [9]. DFT calculations for one-C_6F_6-molecule thick quantum wells, free and supported on a Cu(111) surface, show that the particularly strong intermolecular orbital overlap for the σ^* state is

entirely a molecular property. From its non-nuclear density, we recognize the σ^* wave function as a 2D analogue of 3D SAMOs. Comparing the orbitals and band dispersions of C_6F_6 and C_6H_6, we conclude that SAMOs are a universal feature of flat aromatic molecules; their NFE bands offer a new paradigm for electron transport in organic molecular semiconductors.

The electronic structure of C_6F_6 films on the Cu(111) surface has been studied by 2PP and x-ray spectroscopy [9,26–29]. Angle-resolved 2PP spectra show the LUMO of C_6F_6 forming a highly dispersive band 3.14 eV above E_F with $m_{\mathrm{eff}} = 1.9m_e$ for one monolayer (ML) coverage, decreasing to $1.0m_e$ for 5 ML [9]. Vondrak and Zhu [26] assigned this band to the σ^* state, based on the electronic structure of the free C_6F_6 molecule [30]. Gahl et al. attributed the NFE band formation and adsorption-induced changes in the surface electronic structure to a putative interaction between the σ^* orbitals and image potential (IP) state of a Cu(111) surface [9]. The dielectric continuum model, however, failed to reproduce the 3D band formation of multilayer C_6F_6 films [9]. Most recently, in a study focused on the electronic relaxation within C_6F_6 quantum wells, Föhlisch et al. reassigned the NFE band to the π^* state of C_6F_6 because the core C1s excitation spectra found it below the σ^* state [29]. Similarly, they attributed the NFE properties to mixing of the π^* and the IP state.

We perform structural and spectroscopic measurements on a C_6F_6/Cu(111) surface in an Omicron LT-STM cooled to 5 K and with base pressure below 10^{-10} mbar. A Cu(111) crystal is cleaned by cycles of Ar^+ sputtering and annealing to ~600 K. Hexafluorobenzene is purified by freeze-pump-thaw cycles and dosed through a stainless steel tube onto the Cu(111) surface held at 10 K. Imaging and spectroscopy are carried out in the constant-current and constant-current distance-voltage modes. Low currents (6–20 pA) minimize the tunneling electron-induced diffusion or chemical reaction of the adsorbed molecules [31].

Figures 1(a) and 1(b) show low and high resolution STM images of fractal C_6F_6 islands on the Cu(111) substrate at 10 K, which forms through the limited mobility of molecules along the island edges. Upon annealing the crystal to ~80 K [Fig. 1(c)], the islands coalesce into the close-packed hexagonal (3×3) superlattice with 0.77 nm intermolecular spacing.

To probe the intermolecular interactions of the σ^* state, we measure distance-voltage spectra above selected C_6F_6 molecules within the fractal islands. Figure 2(a) shows numerically differentiated distance voltage spectra (dz/dV) [31], measured above several C_6F_6 molecules with a different number of near neighbors for a compact monolayer as well as fractal islands. The tunneling spectrum for the C_6F_6 monolayer shows a sharp resonance at 3.5 eV above E_F, which we attribute to the σ^* derived LUMO band, reported in 2PP spectra at 3.14 eV [9,26]. Perturbation of the surface field by the STM tip causes the σ^* state to appear in dz/dV spectra at a higher energy [31,32].
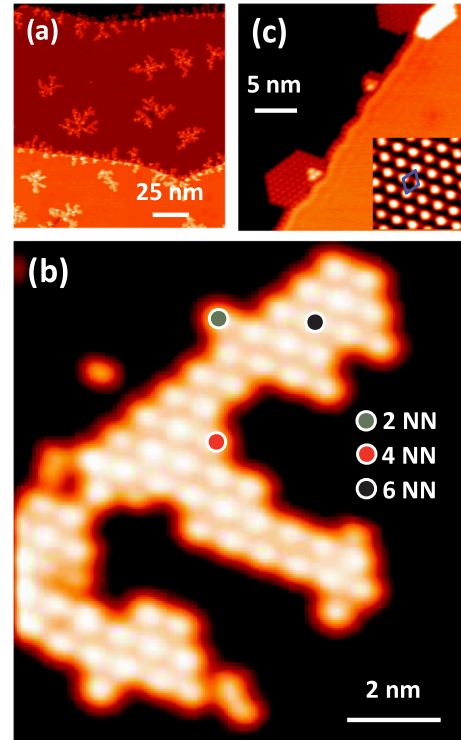
FIG. 1 (color online). (a) STM image $(200 \times 200$ nm, $+0.3$ V, 0.025 nA) of submonolayer C_6F_6 deposited onto a Cu(111) surface held at 10 K. (b) Enlarged image of a fractal island $(27 \times 27$ nm, $+0.2$ V, 0.1 nA) with specific molecules with 2, 4, and 6 NN indicated by colored dots, for which the dz/dV measurements are performed. (c) An image of compact hexagonal C_6F_6 islands after annealing the sample to 80 K. The enlarged image in the inset shows the (3×3) overlayer structure and the surface unit cell with 0.77 nm dimensions.

Using the submolecular resolution of STM, we characterize how the intermolecular interactions modify the properties of the σ^* state by quantifying its energy shift with the number of near-neighbor C_6F_6 molecules within fractal islands. The ramified shape of fractal islands creates variability in the local molecular coordination. Within the STM image in Fig. 1(b) we indicate specific molecules with 2, 4, and 6 near neighbors (NN), where some of the measurements are performed. The dz/dV curves in Fig. 2(a), obtained by averaging measurements at several sites with different molecular environments, show the stabilization of the σ^* state with the NN coordination. The experimental shifts of the σ^* state energy from the isolated molecule to compact monolayer are plotted in Fig. 2(b). We use the tight binding model to simulate the stabilization of the σ^* state through NN interactions using a hopping integral of $\beta = 28$ meV, and assume that the interaction with the next-nearest neighbors decreases as βd^{-2} with the geometrical distance d [33]. The observed stabilization is consistent with an intermolecular wave function overlap of the σ^* state increasing electron delocalization over the molecular quantum well as the coordination number increases.

(a)

(b)
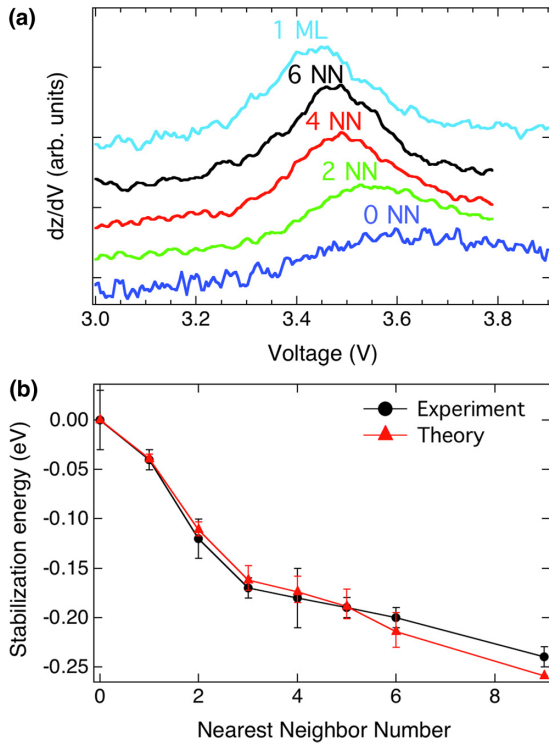
FIG. 2 (color online).   (a) Several dz/dV spectra from isolated molecule to one monolayer coverage spanning the range of C_6F_6 aggregation for different numbers of nearest neighbors. (b) The experimentally observed stabilization energy relative to an isolated molecule from the data in (a). The theoretical stabilization energy is calculated by the tight binding model for fractal islands consisting of 28–66 molecules.

To understand the intermolecular interactions that enable the σ^* state to form the NFE band, we perform DFT calculations for both a free and Cu(111) substrate-supported C_6F_6 monolayer corresponding to the experimental 3×3 superlattice [34–39], with molecules rotated to minimize the F atom repulsion [28]. To account for the Van der Waals interaction, the C_6F_6/Cu(111) structure is calculated with the DFT-D approach adding a semiempirical dispersion potential to the Kohn-Sham DFT energy [40]. This calculation gives a binding energy of 0.63 eV and a height of 3.08 Å primarily due to the dispersion forces. The electronic properties of the supported overlayer depend weakly on the adsorption height because the interaction is through dispersive forces. The DFT calculations give the LUMO bandwidths of 0.66 and 0.65 eV for the supported and the unsupported C_6F_6 monolayer; the negligible enhancement by the substrate indicates that the band formation stems from *intrinsic* electronic interactions among the σ^* orbitals. For comparison, the bandwidth from the tight binding calculation is 0.55 eV. Although σ^* LUMO band crosses the unoccupied part of the Shockley surface state, which undergoes band folding by the (3×3) superlattice, the weak interaction characterized by gaps of <0.1 eV hardly perturbs the σ^* band as compared with the unsupported monolayer.

Figure 3 shows the calculated energy-momentum dispersions and orbital density distributions of bands formed by the σ^*, the highest occupied molecular orbital (HOMO) π, and lowest unoccupied π^* orbitals of the free C_6F_6 quantum well. The calculated $m_{eff} = 2m_e$ and strong orbital delocalization shows that the σ^* band possesses special electronic properties *distinct from* the energetically proximate π states. Contrary to the assignment in Ref. [29], the NFE band cannot be attributed to the π^* state, because its $m_{eff} = -80m_e$ has the opposite sign and very different magnitude than for σ^*. Neither the σ^* nor the π^* states can be modified through interaction with the IP states of the substrate, as suggested previously [9,29]; a constant potential parallel to the surface cannot affect the σ^* or π^* orbital interactions.

To illuminate the special properties of the σ^* state, in Fig. 4 we present the energies and wave functions for valence states of the isolated C_6F_6 molecule. We label the wave functions according to a natural set of quantum
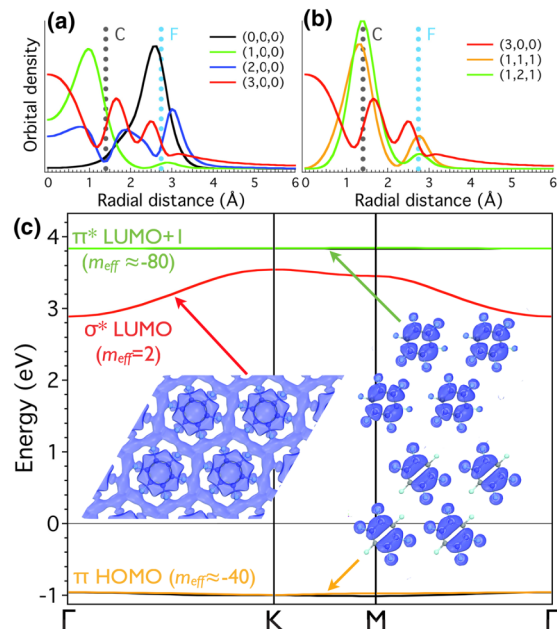
FIG. 3 (color online).   (a) The radial distributions of the $N = (0 - 3, 0, 0)$ probability densities averaged over the azimuthal and surface normal coordinates, showing the increasing superatom character as n_r is increased. The locations of C and F atoms are indicated. The characteristic properties of SAMOs include dominant non-nuclear probability density within the hollow ring and beyond the F atom perimeter, as well as density minima on C and F atoms. (b) The comparison of the probability densities of the superatom σ^* LUMO, with the aromatic π and π^* HOMO and LUMO + 1. Unlike the σ^* orbital, the π orbitals are localized on C and F atoms. (c) The calculated band dispersions for HOMO, LUMO, and LUMO + 1. The π ($m_{eff} = -40m_e$) and π^* ($m_{eff} = -80m_e$) bands are essentially dispersionless, whereas σ^* ($m_{eff} = 2m_e$) has NFE character. The orbital densities for the three bands contrast the large intermolecular density for σ^* with the localized character of π and π^*. Only one component of each doubly degenerate π orbitals is shown.
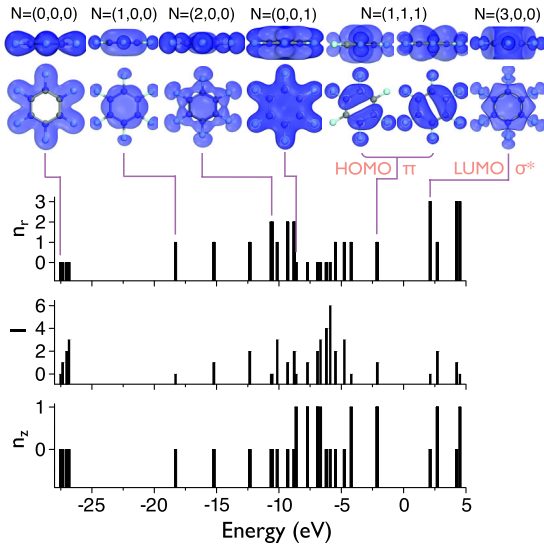
FIG. 4 (color online).   The calculated energy level diagram and molecular orbitals of isolated C_6F_6. The energy distribution of the n_r, l, and n_z quantum numbers is shown separately. Side and top views labeled by quantum numbers $N = (n_r, l, n_z)$ are shown for the orbitals in Figs. 3(a) and 3(b).

numbers for the D_{6h} molecular symmetry, which clarify the features of molecular wave functions that promote the NFE band formation. Quantum numbers n_r, l, and n_z respectively, count the number of nodal surfaces normal to the molecular plane, extending radially from the center and upon 2π azimuthal rotation, and in the molecular plane. Accordingly, the σ^* state with three radial nodes is described by $N = (n_r, l, n_z) = (3, 0, 0)$. In Fig. 4, we sort the electronic states of C_6F_6 as a function of energy according to this scheme and show the calculated probability density isocontours for selected orbitals. We emphasize the a_{1g} symmetry orbitals forming the progression $N = (0–3, 0, 0)$, because for a given "principal" quantum number n_r they have the strongest intermolecular orbital hybridization. Figures 3(a) and 3(b) show the radial cross sections of $N = (0–3, 0, 0)$ wave functions after averaging over the azimuthal and surface normal coordinates, and contrast them with those of the weakly dispersive π-symmetry HOMO [$N = (1, 1, 1)$], and LUMO + 1 orbitals [$N = (1, 2, 1)$]. For the $N = (0–3, 0, 0)$ sequence, increasing n_r causes the probability density to spread from the C and F atoms into non-nuclear regions corresponding to the hollow center and perimeter of the C_6F_6 molecule. From the cross sections in Fig. 3, we conclude that the primary origin of the hybridization of the σ^* state into the NFE quantum well band is its substantial non-nuclear density beyond the F atom perimeter. By contrast, the π and π^* wave functions are firmly localized on the C and F atoms [28]. The back donation from F atom $2p$ orbitals to the aromatic ring π orbitals [28] further diminishes the in-plane intermolecular interactions among the π orbitals. The propensity of the σ orbitals to acquire

non-nuclear density at a lower energy than the π orbitals explains why they readily form the delocalized bands.

Having explained the origin of the NFE band, we consider the broader context of our analysis. We find that the tendency of an orbital of a planar molecule to form a dispersive band is defined by the value of its n_r quantum number. Introducing angular or in-plane nodes increases the electron kinetic energy and localization; therefore, a_{1g} orbitals within an n_r shell have the strongest intermolecular hybridization. Indeed, for the benzene molecule (C_6H_6) chemisorbed flat on the Ni(110) surface, the occupied $N = (1, 0, 0)$ state also forms a strongly dispersive band 10.9 eV below E_F [25]. Such σ interactions have been predicted to lead to C_6H_6 metallization of compressed planar 2D layers [5]. These interactions between planar molecules cannot be attributed to mediation by F or H atoms but rather the propensity of σ orbitals to displace electron density to the molecule periphery as n_r increases.

Our finding has broad implications for designing the electronic properties of aromatic molecular solids. The spread of $N = (n_r, 0, 0)$ wave functions into the non-nuclear regions with increasing n_r is the defining feature of SAMOs of hollow molecules. We argue that with increasing n_r molecular orbitals of planar hollow molecules gain 2D superatom character, which enables the NFE band formation. These bands are tunable by molecular design as evident from the comparison between the (3,0,0) and (1,0,0) states of C_6F_6 and C_6H_6. Fluorine atoms of C_6F_6, being σ acceptors and π donors, withdraw charge from the aromatic ring [28,41]. Hence, the C-F dipoles locate net positive charge on the hollow ring, which attracts the σ^* state orbital density to the center, but some density also spills out to the perimeter. The positive dipole potential at the center stabilizes the σ^* state with a SAMO character below the π^* state. By contrast, for benzene, the internal C-H dipoles have the opposite polarity and therefore displace orbital density to the perimeter, making the corresponding $N = (n_r, 0, 0)$ molecular orbitals more diffuse than for C_6F_6 and raising the energy σ^* above π^*. The superatom character, being a manifestation of the exchange-correlation and dipole potentials, is not strongly sensitive to reduction of symmetry by substituting F or H atoms by another functional group.

Thus, modifying the central potential by charge transfer between the molecular center and periphery, or by introducing a central metallic cation, are possible strategies for designing the electronic properties of SAMOs within 2D molecules. In the case of fullerenes and nanotubes, we have shown that the choice of endohedral atoms or clusters can be used to control the energy of SAMOs in hollow molecules [18,19,24]. We expect that the facility of synthesizing 2D hollow molecules, together with our simple principles for the SAMO stabilization, will enable the discovery of other strong band forming organic materials with promising charge transport properties.

---

*Present address: Department of Physics, North Carolina State University, Raleigh, NC 27695, USA.

†Present address: Department of Chemistry, University of Virginia, Charlottesville, VA 22904, USA.

‡Corresponding authors.
petek@pitt.edu
zhaojin@ustc.edu.cn

[1] V. Coropceanu, J. Cornil, D. A. da Silva Filho, Y. Olivier, R. Silbey, and J. L. Bredas, Chem. Rev. **107**, 926 (2007).

[2] S. Kera, H. Yamane, and N. Ueno, Prog. Surf. Sci. **84**, 135 (2009).

[3] N. Koch, A. Vollmer, I. Salzmann, B. Nickel, H. Weiss, and J. P. Rabe, Phys. Rev. Lett. **96**, 156803 (2006).

[4] H. Kakuta, T. Hirahara, I. Matsuda, T. Nagao, S. Hasegawa, N. Ueno, and K. Sakamoto, Phys. Rev. Lett. **98**, 247601 (2007).

[5] X.-D. Wen, R. Hoffmann, and N. W. Ashcroft, J. Chem. Soc. **133**, 9023 (2011).

[6] H. Yamane, S. Kera, K. K. Okudaira, D. Yoshimura, K. Seki, and N. Ueno, Phys. Rev. B **68**, 033102 (2003).

[7] X. Feng, V. Marcon, W. Pisula, M. R. Hansen, J. Kirkpatrick, F. Grozema, D. Andrienko, K. Kremer, and K. Müllen, Nat. Mater. **8**, 421 (2009).

[8] Q. Li, C. Han, S. R. Horton, M. Fuentes-Cabrera, B. G. Sumpter, W. Lu, J. Bernholc, P. Maksymovych, and M. Pan, ACS Nano **6**, 566 (2012).

[9] C. Gahl, K. Ishioka, Q. Zhong, A. Hotzel, and M. Wolf, Faraday Discuss. **117**, 191 (2000).

[10] R. Temirov, S. Soubatch, A. Luican, and F. S. Tautz, Nature (London) **444**, 350 (2006).

[11] C. H. Schwalb, S. Sachs, M. Marks, A. Scholl, F. Reinert, E. Umbach, and U. Höfer, Phys. Rev. Lett. **101**, 146801 (2008).

[12] M. Feng, J. Zhao, and H. Petek, Science **320**, 359 (2008).

[13] B. W. Heinrich, L. Limot, M. V. Rastei, C. Iacovita, J. P. Bucher, D. M. Djimbi, C. Massobrio, and M. Boero, Phys. Rev. Lett. **107**, 216801 (2011).

[14] X. Y. Zhu, G. Dutton, D. P. Quinn, C. D. Lindstrom, N. E. Schultz, and D. G. Truhlar, Phys. Rev. B **74**, 241401 (2006).

[15] N. L. Zaitsev, I. A. Nechaev, P. M. Echenique, and E. V. Chulkov, Phys. Rev. B **85**, 115301 (2012).

[16] L. Chen, H. Li, and A. T. S. Wee, Phys. Rev. Lett. **105**, 226103 (2010).

[17] P. Han and P. S. Weiss, Surf. Sci. Rep. **67**, 19 (2012).

[18] J. Zhao, M. Feng, J. Yang, and H. Petek, ACS Nano **3**, 853 (2009).

[19] T. Huang, J. Zhao, M. Feng, H. Petek, S. Yang, and L. Dunsch, Phys. Rev. B **81**, 085434 (2010).

[20] M. Feng, J. Zhao, T. Huang, X. Zhu, and H. Petek, Acc. Chem. Res. **44**, 360 (2011).

[21] J. O. Johansson, G. G. Henderson, F. Remacle, and E. E. B. Campbell, Phys. Rev. Lett. **108**, 173401 (2012).

[22] W. Chan, J. Tritsch, A. Dolocan, M. Ligges, L. Miaja-Avila, and X. Zhu, J. Chem. Phys. **135**, 031101 (2011).

[23] Y. Pavlyukh and J. Berakdar, J. Chem. Phys. **135**, 201103 (2011).

[24] S. Hu, J. Zhao, Y. Jin, J. Yang, H. Petek, and J. G. Hou, Nano Lett. **10**, 4830 (2010).

[25] W. Huber, M. Weinelt, P. Zebisch, and H. P. Steinrück, Surf. Sci. **253**, 72 (1991).

[26] T. Vondrak and X. Y. Zhu, J. Phys. Chem. B **103**, 3449 (1999).

[27] K. Ishioka, C. Gahl, and M. Wolf, Surf. Sci. **454–456**, 73 (2000).

[28] S. Vijayalakshmi, A. Föhlisch, P. S. Kirchmann, F. Hennies, A. Pietzsch, M. Nagasono, and W. Wurth, Surf. Sci. **600**, 4972 (2006).

[29] A. Föhlisch, S. Vijayalakshmi, A. Pietzsch, M. Nagasono, W. Wurth, P. S. Kirchmann, P. A. Loukakos, U. Bovensiepen, M. Wolf, M. Tchaplyguine, and F. Hennies, Surf. Sci. **606**, 881 (2012).

[30] T. M. Miller, J. M. V. Doren, and A. A. Viggiano, Int. J. Mass Spectrom. **233**, 67 (2004).

[31] D. B. Dougherty, P. Maksymovych, J. Lee, and J. T. Yates, Jr., Phys. Rev. Lett. **97**, 236806 (2006).

[32] A. Pronschinske, D. J. Mardit, and D. B. Dougherty, Phys. Rev. B **84**, 205427 (2011).

[33] See Supplemental Material at http://link.aps.org/supplemental/10.1103/PhysRevLett.109.266802 for detailed information on the tight binding and DFT band structure calculations.

[34] We performed plane-wave basis set DFT electronic structure calculations with a cutoff energy of 400 eV using the generalized gradient approximation with the PBE functional as implemented in the Vienna *ab initio* simulation package (VASP). The projector augmented wave method was used to describe the electron-ion interaction. The surface is simulated with a six-layer Cu atom slab with C_6F_6 placed on one side with dipole moment correction and 1.5 nm vacuum.

[35] G. Kresse and J. Hafner, Phys. Rev. B **48**, 13 115 (1993).

[36] G. Kresse and J. Hafner, Phys. Rev. B **47**, 558 (1993).

[37] G. Kresse and J. Hafner, Phys. Rev. B **49**, 14 251 (1994).

[38] J. P. Perdew, K. Burke, and M. Ernzerhof, Phys. Rev. Lett. **77**, 3865 (1996).

[39] G. Kresse and D. Joubert, Phys. Rev. B **59**, 1758 (1999).

[40] X. Wu, M. C. Vargas, S. Nayak, V. Lotrich, and G. Scoles, J. Chem. Phys. **115**, 8748 (2001).

[41] T. X. Carroll, T. D. Thomas, H. Bergersen, and K. J. Børve, J. Org. Chem. **71**, 1961 (2006).